International Journal of Heat and Mass Transfer 52 (2009) 5895–5908

Contents lists available at ScienceDirect

International Journal of Heat and Mass Transfer

journal homepage: www.elsevier.com/locate/ijhmt

Hydromagnetic free convection of a radiating fluid

Cho Young Han *

Satellite Thermal & Propulsion Department, Satellite Technology Division, Satellite Research & Development Head Office, Korea Aerospace Research Institute, 115 Gwahangno, Yuseong-gu, Daejeon 305-333, Republic of Korea

ARTICLE INFO

Article history:
Received 11 May 2009
Received in revised form 10 August 2009
Accepted 10 August 2009
Available online 12 September 2009

Keywords:
Hydromagnetic flow
Natural convection
Radiation heat transfer
Magnetic field
Radiating fluid

ABSTRACT

Natural convection of an electrically conducting and radiating fluid in the presence of an external magnetic field is investigated numerically. The two opposing side walls are differentially heated with a temperature difference specified, while the top and bottom walls are insulated. The coupled momentum and energy equations associating with the electromagnetic retarding force as well as the buoyancy force terms are solved by an iterative procedure using the SIMPLER algorithm based on control volume approach. Steady-state conditions are assumed. The finite-volume method is utilised to solve the radiation transport adopting the same computational grid as used in solving the flow field, with which the radiating fluids in an enclosure are assumed to be radiatively opaque, transparent and participating, respectively. After validating the numerical procedures, the changes in the buoyant flow patterns and temperature distribution affected by combined radiation and a magnetic field are focused mainly. Comparative results for the velocity profiles and the heat transfer rates are presented too. Based on the results of this study, it was found that the radiation played a significant role in developing the hydromagnetic free convective flow in a differentially heated enclosure.

1. Introduction

Hydromagnetic flow and heat transfer problems have received considerable attention in years, as their applications reside in many industrial fields. The most common type of body force, which acts on fluid, is attributed to gravity so that the body force vector can be deduced from the gravitational acceleration. On the other hand, when an electrically conducting fluid is subjected to a magnetic field, the fluid motion induces an electric current such that the fluid velocity is reduced on account of interaction between the electric current and the fluid motion. In this context, there exist two body forces, i.e., buoyancy and Lorentz forces, in case of the free convection of an electrically conducting fluid in the presence of a magnetic field. They interact with each other, and in turn influence the transport phenomena of heat and mass.

Among various studies for MHD free flows, rather small amount of studies have been accomplished for the confined enclosures. Seki et al. [1] studied the laminar natural convection of mercury subjected to a magnetic field parallel to gravity in a rectangular enclosure. Numerical results were found and compared to their experiment with which considered a partially heated vertical wall by a uniform heat generator. The effect of direction of an external magnetic field on a low Prandtl number fluid in a cubical enclosure was numerically examined by Ozoe and Okada [2]. Rudraiah et al. [3] performed a numerical simulation about natural convection in a two-dimensional cavity filled with an electrically conducting fluid in the presence of a magnetic field aligned to gravity. They selected the Grashof and Hartmann numbers as controlling parameters to examine the effect of a magnetic field on free convection and associated heat transfer. On the other hand Bessaih et al. [4] studied the buoyancy-induced flow of gallium in cavities simulating the apparatus for crystal growth. The combined effect on the flow structure of wall electrical conductivity and magnetic field orientation were numerically investigated in their work. The three-dimensional free convective flow in a cubical enclosure in the presence of a transverse magnetic field was analysed by Kolsi et al. [5] numerically.

Recently many researchers have taken an interest in the effect of thermal radiation on the hydromagnetic flow and heat transfer problems, by reason of its great importance in industrial fields. Radiation effect can be quite significant at high operating temperature. Many processes in engineering areas occur at high temperatures and the knowledge of radiation heat transfer becomes very important for the design of pertinent equipments. The radiative flows of an electrically conducting fluid with high temperature in the presence of a magnetic field are encountered in various propulsion devices for satellites and interplanetary spacecrafts, electrical power generation, astrophysical flows, solar power technology, space vehicle re-entry, nuclear engineering applications and other industrial areas. The effects of thermal radiation on hydromagnetic boundary layer flows were studied by

* Tel.: +82 42 860 2033; fax: +82 42 860 2603.
E-mail address: cyhan@hanmir.com

0017-9310/$ - see front matter © 2009 Elsevier Ltd. All rights reserved.
doi:10.1016/j.ijheatmasstransfer.2009.08.010

Nomenclature

A	aspect ratio, $A = H/L$
B_o	applied magnetic field [T]
$\overline{B}^*$	dimensionless radiation temperature, $\overline{B}^* = T/T_o = T^*\delta + 1$
g	gravitational acceleration [m s^{-2}]
G	incident radiation, $G = \int_{4\pi} I d\Omega$
Gr	Grashof number, Gr = Ra/Pr
H	enclosure height [m]
$H(\vec{r})$	irradiation [W m^{-2}]
Ha	Hartmann number, $Ha = B_o L\sqrt{\sigma/\mu}$
I	radiation intensity [W m^{-2} Sr^{-1}]
L	enclosure width [m]
$\hat{n}$	unit normal vector
N	conduction-radiation parameter, $N = \mathrm{Pl}\cdot\tau$
Nu	Nusselt number
Pl	Planck number, $\mathrm{Pl} = (k/L)/(4\bar{\sigma}T_o^3)$
Pr	Prandtl number, $\mathrm{Pr} = \nu/\alpha$
q	local heat flux [W m^{-2}]
$\vec{r}$	position vector
Ra	Rayleigh number, $Ra = g\bar{\beta}\Delta T L^3/(\nu\alpha)$
s	distance travelled by ray [m]
$\hat{s}$	unit direction vector
T	temperature [K]
T_C, T_H	cooled and heated isothermal wall temperature [K]
T_o	reference temperature, $T_o = (T_H + T_C)/2$
u, v	velocity components in x and y directions [ms^{-1}]
u_o	reference velocity, $u_o = \alpha/L$
x, y	Cartesian coordinates

Greek symbols

α	thermal diffusivity [m^2 s^{-1}]
β	extinction coefficient, $\beta = \kappa_a + \sigma_s [m^{-1}]$
$\bar{\beta}$	volumetric expansion coefficient [K^{-1}]
δ	overheat ratio, $\delta = (T_H - T_C)/T_o$
ε	emissivity
θ	polar angle [rad]
κ_a	absorption coefficient [m^{-1}]
μ	dynamic viscosity [kg m^{-1} s^{-1}]
ν	kinematic viscosity [m^2 s^{-1}]
ρ	density [kg m^{-3}]
σ	electrical conductivity [Ω^{-1} m^{-1}]
$\bar{\sigma}$	Stefan-Boltzmann constant [5.67×10^{-8} W m^{-2} K^{-4}]
σ_s	scattering coefficient [m^{-1}]
τ	optical thickness, $\tau = \beta L$
ϕ	azimuthal angle [rad]
Φ	scattering phase function [Sr^{-1}]
Ψ	stream function
ω	scattering albedo, $\omega = \sigma_s/\beta$
Ω	solid angle [Sr]

Superscripts

C	conduction
R	radiation
T	total quantity
$*$	dimensionless quantities
$'$	incoming direction

Subscripts

0	reference quantities
C	cooled wall
H	heated wall
w	wall

Chamkha [6], Seddeek [7], Ghaly [8] and Raptis et al. [9]. Mahmud and Fraser [10] examined analytically radiation effects on mixed convection through a vertical channel in the presence of a transverse magnetic field.

In terms of the radiation treatment, however, all investigators abovementioned have taken advantage of quite simple approximations for the convenience of the analysis. Most of them, for example Refs. [6,8,9], evaluated the divergence of radiative heat flux by using the optically thick approximation, i.e., Rosseland approximation, so that they converted the complex radiation problem to the simpler conduction one accounting for the radiation conductivity. The main drawback of this sort of approach is that it causes substantial error in the radiation heat flux near the radiation boundary. On the other hand Seddeek [7] studied the radiation effect on the free convection of a hydromagnetic fluid over the semi-infinite flat plate incorporating the optically thin medium. He supposed that the medium did not carry out any self-absorption but it absorbed the radiation emitted from the boundary. Mahmud and Fraser [10] employed the two-flux simplification [11] for their radiation model.

The radiation effect, in general, affects on the natural convection rather than the forced convection. The main reason comes from the intrinsic relation between the thermal field and the flow regime. In case of the natural convection problem, radiation effect is directly associated with the energy equation by means of a radiation source term. After solving the energy equation we can get to know the temperature field. It is very important, in consequence, to evaluate the radiation source term accurately, as the density difference due to temperature distribution causes the occurrence of buoyancy force, especially in the natural convection phenomena. For that reason proper modelling as well as accurate solving technique for radiation, are prerequisite for those analyses.

The main objective of this investigation is to examine the effects of thermal radiation on thermo-fluid dynamics behaviour in an enclosure filled with the electrically conducting fluid under the influence of a magnetic field. Different from the previous studies the two-dimensional analysis is performed rather than dealing the boundary layer type of analysis adopting similarity transformation as a sort of the one-dimensional analysis. Moreover the efficient and accurate multi-flux method to solve the radiative transfer equation (RTE) is incorporated into the present analysis instead of using simple approximations not to solve the RTE or just introducing two-flux method with very low accuracy. As a result, after confirming the numerical results without radiation, the effects of combined radiation and a magnetic field on the thermo-fluid dynamics characteristics as well as associated heat transfer, are analysed and discussed in detail.

2. Analysis model

For many electrically conducting fluids used in laboratories, the electrical conductivity is usually small. Subsequently the magnetic Reynolds number should be very small. Therefore it is reasonable to assume that the induced magnetic field by the motion of the electrically conducting fluid is negligible compared to the external magnetic field applied. Based on this assumption the electromagnetic retarding force and the buoyancy force terms are appeared in the horizontal and vertical momentum equations respectively, such that the governing equations are not amenable to the bound-

ary layer type of analysis. In this simulation the SIMPLER algorithm [12] is involved to estimate the flow field, which is numerically stable and being widely used. The resultant solution of the governing equations is to be proposed associating with the finite volume method (FVM) [13] that is the multi-flux method to solve the RTE. The effect of controlling parameters pertaining to fluid flow, heat transfer characteristics and radiation properties is evaluated numerically.

2.1. Governing equations

A schematic of the two-dimensional rectangular enclosure with width L and height H is shown in Fig. 1. It is filled with the electrically conducting fluid that is viscous and incompressible. While the medium within the enclosure is assumed to be gray and it absorbs, emits and scatters the radiation. The left- and right-hand-side walls are kept at T_C and T_H, respectively. The ceiling and floor are assumed to be insulated for both conduction and radiation. All four walls of the enclosure are black and diffuse.

The fluid is permeated by the uniform magnetic field B_o aligned with gravity. In addition the induced electric current does not distort considerably the magnetic field applied. The fluid properties including the electrical conductivity are assumed to be constant except for the density, so that the Boussinesq approximation is used. Neglecting viscous and ohmic dissipations, the governing equations for mass, momentum, energy and radiation heat transfer of the steady laminar flow are as follows.

Continuity

$$\frac{\partial u}{\partial x}+\frac{\partial v}{\partial y}=0 \tag{1}$$

X-momentum

$$\frac{\partial}{\partial x}(u^2)+\frac{\partial}{\partial y}(uv)=-\frac{1}{\rho}\frac{\partial p}{\partial x}+\nu\nabla^2 u-\frac{\sigma B_o^2}{\rho}u \tag{2}$$

Y-momentum

$$\frac{\partial}{\partial x}(uv)+\frac{\partial}{\partial y}(v^2)=-\frac{1}{\rho}\frac{\partial p}{\partial y}+\nu\nabla^2 v+g\bar{\beta}(T-T_o) \tag{3}$$

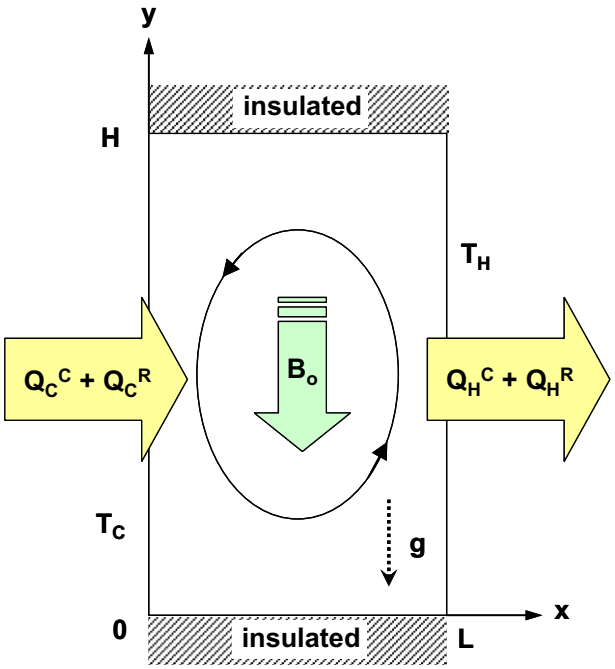

Fig. 1. Schematic diagram of the two-dimensional enclosure.

Energy

$$\frac{\partial}{\partial x}(uT)+\frac{\partial}{\partial y}(vT)=\alpha\nabla^2 T-\nabla\cdot q^R \tag{4}$$

Radiative transfer equation

$$\frac{dI}{ds}=\kappa_a\frac{\bar{\sigma}T^4}{\pi}-\beta I+\frac{\sigma_s}{4\pi}\int_{4\pi} I'\Phi d\Omega' \tag{5}$$

In the above equations, u and v are the velocity component in the x and y directions. The pressure, temperature and radiation intensity are denoted by p, T and I, respectively. The relevant fluid properties are kinematic viscosity ν, thermal diffusivity α, electrical conductivity σ and volumetric expansion coefficient $\bar{\beta}$. The other properties for radiation are absorption coefficient κ_a, Stefan-Boltzmann constant $\bar{\sigma}$, extinction coefficient β and scattering coefficient σ_s. The Φ in Eq. (5) designates the scattering phase function. The governing equations are nondimensionalised using the following variables:

$$X^*=x/L,\ y^*=y/L,\ u^*=u/u_o,\ v^*=v/u_o \tag{6}$$

$$p^*=\frac{p}{\rho_o u_o^2},\ T^*=\frac{T-T_o}{T_H-T_C},\ \bar{B}^*=\frac{T}{T_o}=T^*\delta+1 \tag{7}$$

$$\beta=\kappa_a+\sigma_s,\ \tau=\beta L,\ \omega=\sigma_s/\beta,\ I^*=\frac{I}{\bar{\sigma}T_o^4},\ G^*=\int_{4\pi} I^* d\Omega \tag{8}$$

$$\mathrm{Pr}=\nu/\alpha,\ Ra=\frac{g\bar{\beta}\Delta TL^3}{\nu\alpha},\ Gr=Ra/\mathrm{Pr},\ Ha=B_oL\sqrt{\frac{\sigma}{\mu}},$$
$$Pl=\frac{k/L}{4\bar{\sigma}T_o^3} \tag{9}$$

The reference velocity is defined as $u_o=\alpha/L$. The overheat ratio is expressed by $\delta=(T_H-T_C)/T_o$, while the reference temperature is defined as the arithmetic mean of the two isothermal wall temperatures, i.e., $T_o=(T_H+T_C)/2$. The dimensionless radiation temperature $\bar{B}^*$ is introduced to nondimensionalise the RTE, and it is the function of the overheat ratio. Based on the presumptions above, the dimensionless governing equations can be shown as follows.

Continuity

$$\frac{\partial u^*}{\partial x^*}+\frac{\partial v^*}{\partial y^*}=0 \tag{10}$$

X-momentum

$$\frac{\partial}{\partial x^*}(u^{*2})+\frac{\partial}{\partial y^*}(u^*v^*)=-\frac{\partial p^*}{\partial x^*}+\mathrm{Pr}\nabla^2 u^*-u^*\mathrm{Pr}Ha^2 \tag{11}$$

Y-momentum

$$\frac{\partial}{\partial x^*}(u^*v^*)+\frac{\partial}{\partial y^*}(v^{*2})=-\frac{\partial p^*}{\partial y^*}+\mathrm{Pr}\nabla^2 v^*+Gr\mathrm{Pr}^2T^* \tag{12}$$

Energy

$$\frac{\partial}{\partial x^*}(u^*T^*)+\frac{\partial}{\partial y^*}(v^*T^*)=\nabla^2T^*-\frac{1}{\delta}\frac{\tau}{Pl}(1-\omega)\left(\bar{B}^{*4}-\frac{1}{4}G^*\right) \tag{13}$$

Radiative transfer equation

$$\frac{1}{\tau}\frac{dI^*}{ds^*}=\frac{(1-\omega)}{\pi}\bar{B}^{*4}-I^*+\frac{\omega}{4\pi}\int_{4\pi} I'^*\Phi d\Omega' \tag{14}$$

2.2. Dimensionless boundary conditions

The boundary conditions for diffusely reflecting and emitting isothemal opaque walls are as follows:

$$u^*=v^*=0,\ T^*=-0.5 \text{ at } x^*=0 \tag{15}$$
$$u^*=v^*=0,\ T^*=0.5 \text{ at } x^*=1 \tag{16}$$

$$I^*(\vec{r}_w,\hat{s}) = \frac{\varepsilon_w}{\pi}\bar{B}_w^{*4} + \frac{1-\varepsilon_w}{\pi}H^*(\vec{r}_w)$$
$$\text{where } H^*(\vec{r}_w) = \int_{\hat{s}'\cdot\hat{n}_w<0} I^*(\vec{r}_w,\hat{s}')|\hat{s}'\cdot\hat{n}_w|d\Omega' \quad (17)$$

Here, ε_w and $\hat{n}_w$ denote the wall emissivity and surface unit normal vector, respectively. $H^*(\vec{r}_w)$ represents the integration of all incoming directional intensities, i.e., the irradiation. Non-slip conditions of the velocities are assigned on the ceiling and floor. The thermal boundary condition at adiabatic ceiling and floor is found from the following energy balancing equation, in which the net radiation into the wall surface is balanced by conductive heat loss from the wall [14]:

$$-\left.\frac{\partial T^*}{\partial y^*}\right|_w + \frac{\varepsilon_w}{4Pl\delta}(\bar{B}_w^{*4} - H^*) = 0 \quad (18)$$

In the above equation the Planck number Pl is selected as the interaction parameter rather than the more commonly used conduction-radiation parameter $N(=\mathrm{Pl}\cdot\tau)$, in order to get rid of the dependency of energy balance on the optical thickness τ at an adiabatic wall.

In some cases, for instance Refs. [15,16], for the benefit of computational easiness, the adiabatic conditions at ceiling and floor are such that the temperature gradients at adiabatic walls are set to be just zero assuming perfectly reflecting walls, even when incorporating the radiation heat transfer. As a consequence the temperature gradients at the adiabatic walls are never changed from zero, without regard to the radiation involvement. The adiabatic condition applied in this study (Eq. (18)), hence, could simulate more realistic situation in practice, although it is demanding to treat computationally.

2.3. Heat transfer rates

To estimate the heat transfer rates at two isothermal walls, various types of average Nusselt numbers are defined as follows:

$$\overline{Nu}_w^C = \frac{1}{A}\int_0^A q_w^{C^*}dy^* \quad (19)$$

$$\overline{Nu}_w^R = \frac{1}{4Pl\delta}\frac{1}{A}\int_0^A \mathrm{sign}(\hat{n}_w)\cdot q_w^{R^*}dy^* \quad (20)$$

$$\overline{Nu}_w^T = \overline{Nu}_w^C + \overline{Nu}_w^R \quad (21)$$

$$\text{where } q_w^{C^*} = -\left.\frac{dT^*}{dx^*}\right|_w, \quad q_w^{R^*} = \int_{4\pi} I^*(\hat{s}\cdot\hat{n}_w)d\Omega \quad (22)$$

From the above equations, A means the aspect ratio, i.e., $A = H/L$. The conductive and radiative average Nusselt numbers at the walls are represented by $\overline{Nu}_w^C$ and $\overline{Nu}_w^R$, respectively. Their sum, $\overline{Nu}_w^T$ is the total average Nusselt number, which denotes the total amount of heat transfer at the wall. Since the steady state is assumed in this study, the total average Nusselt numbers at both hot and cold walls are same.

3. Numerical analysis

3.1. Numerical method

A numerical analysis of thermo-fluid dynamics characteristics is conducted by adopting the SIMPLER algorithm developed by Patankar [12]. While the convection term is discretised using the QUICK finite-difference scheme [17], the central difference method is chosen for the diffusion term. In order to compute the radiation source term in the energy equation, the dimensionless linearised radiative transfer equation is used here as proposed by Chai et al. [13]. A control-volume surface intensity is evaluated from the nodal point value using a step spatial difference scheme [13] to ensure the positive intensity. After some preliminary calculations for checking convergence and accuracy, the spatial and angular domains are discretised into 51×51 non-uniform control volumes in the x and y directions, and 2×24 control angles with uniform $\Delta\phi$ and $\Delta\theta$ in ϕ and θ directions, respectively. The typical spatial and angular control volumes are presented in Fig. 2.

Computations are proceeded by the following procedures. To begin with, the radiative wall heat fluxes and the source terms in the energy equation are determined by solving the radiative transfer equation. The velocity field is estimated from the momentum equation. After the updated temperature is estimated from the energy equation based on the interior point temperature at the previous iteration, the wall conductive heat fluxes are estimated. Then, these values of the wall conductive heat flux, the irradiation and the surface temperature are used to update the non-prescribed wall surface temperatures by solving the energy balance Eq. (18) with the bisection method. In computation, to reduce the error in the wall conductive heat flux, the grid system should be clustered

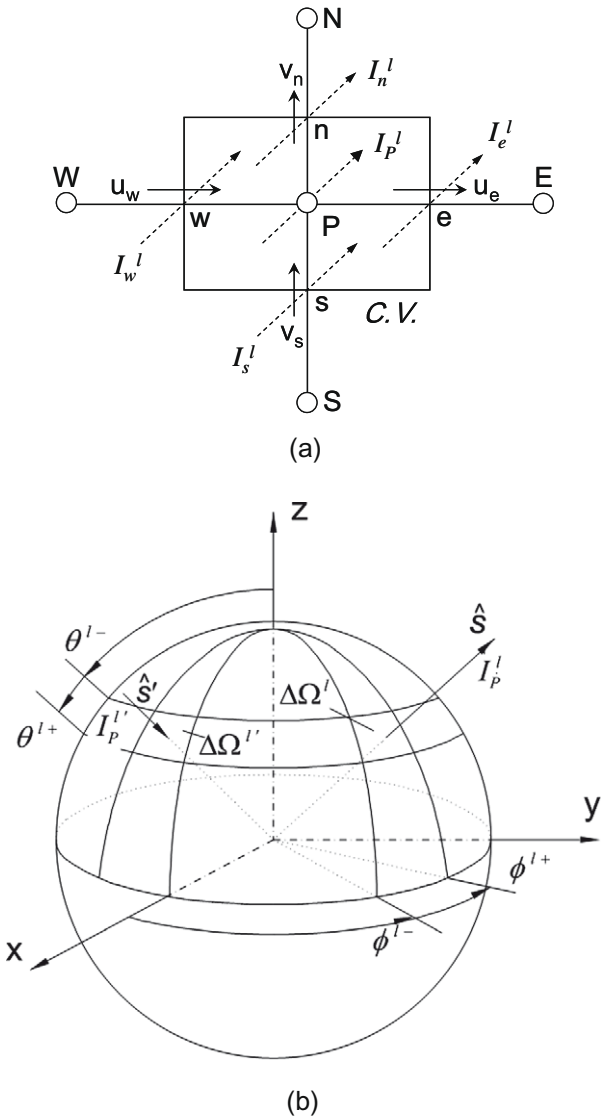

Fig. 2. Typical spatial control volume and control angle: (a) grid layout and typical radiation direction; (b) angular discretisation used.

near the walls. Since the calculation of radiative heat fluxes is not necessarily required at every iteration to produce a reliable steady-state result, the radiative heat flux is updated every ten iterations. However, the wall surface temperature is recalculated and changed at each iteration with an estimated wall conductive heat flux.

Finally, the convergence criteria for main variables are checked if the steady state is reached. Computations are terminated when the difference in total average Nusselt numbers for the hot and cold walls is within less than 10^{-3} to meet the overall energy balance in the enclosure.

$$|\overline{Nu}_H^T - \overline{Nu}_C^T| \le 10^{-3} \tag{23}$$

3.2. Validation of numerical results

The case of pure natural convection is considered for verification in comparison with the experimental results by Linthorst et al. [18] in Fig. 3. They measured the dimensionless vertical velocity by means of the Laser Doppler velocimeter at mid-height of a cavity filled with air. For the computational validation the Rayleigh number is set to 2.2×10^5 as was in the experiment. A square cavity with a length $L = 4$ cm, of which top and bottom walls are thermally insulated, is chosen. The Prandtl number of the air is fixed as 0.733, while the thermal diffusivity is 26.89×10^{-6} m^2/s that is deduced from the mean temperature of the fluid, i.e., 320 K. The overheat ratio is assigned to 2/3 which is the same value being employed in this study. The computational domain is divided by 51×51 non-uniform grids spatially, and the same grids are used for further investigation. The validation results agree very well with the experimental data, regardless of a small deviation displayed in Fig. 3, which may come from the imperfect condition of adiabatic walls in the experiment.

Present method is verified also for the low Prandtl number fluids comparing with the experimental data obtained by Wolff et al. [19], as illustrated in Fig. 4. Free convection in a differentially heated square cavity filled with the liquid gallium (Pr = 0.0208) is considered when Ra = 1.682×10^5. Predicted results are shown in lines and experimental data are represented by symbols in Fig. 4. It shows satisfactory agreement between the predicted and measured temperatures at three different heights. However the numerical results at $y^* = 0.5$ show lower values than the experimental data indicating the presence of stronger natural convection. This may be attributed to the presence of the thermocouple rakes in the liquid gallium, which tend to suppress the flow, as pointed

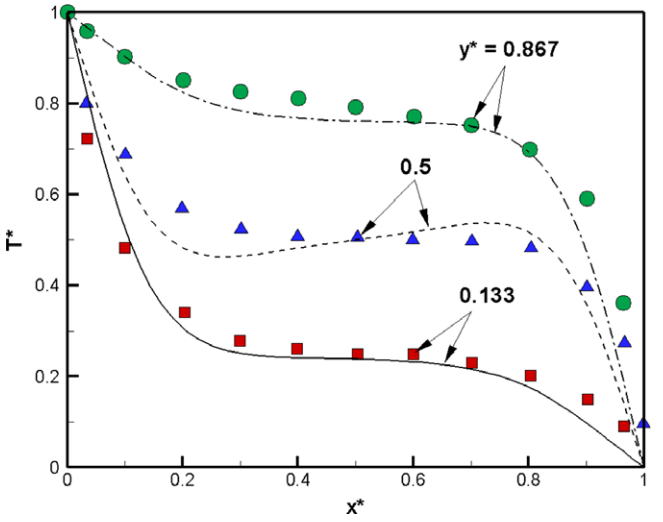

Fig. 4. Predicted and measured temperature profiles at three different heights of the cavity filled with liquid gallium while Ra = 1.682×10^5 and Pr = 0.0208.

out by Wolff et al. [19]. In addition in case of Ra = 3.659×10^5, their temperature profiles measured in the liquid tin (Pr = 0.011) are compared to the predictions, and it is found to be in good agreement too. So it is believed that the present method could be applied to a fluid flow having smaller values of Pr.

In order to validate the present numerical method for radiation also, simulation results for a square cavity of $L \times L$ are compared with those obtained by Chai [20]. Temperatures of left-hand-side wall and floor are T_o, respectively, otherwise the remaining walls are kept at 0 K. The emissivity of the left wall is 0.5, and the other walls are black, i.e., $\varepsilon_w = 1$. The pure absorbing medium ($\tau = 1$, $\omega = 0$) fills this enclosure. The spatial and angular domains are discretised into 22×23 non-uniform control volumes in the x and y directions and 2×24 control angles with uniform $\Delta\phi$ and $\Delta\theta$ in ϕ and θ angular directions, respectively. The present results for incident radiation ($G^*/4$) depicted in solid lines are in good agreement with the previous ones obtained by Chai [20] being symbolised, as shown in Fig. 5.

Supplementary validity of present numerical technique for combined radiation and natural convection in a radiatively active

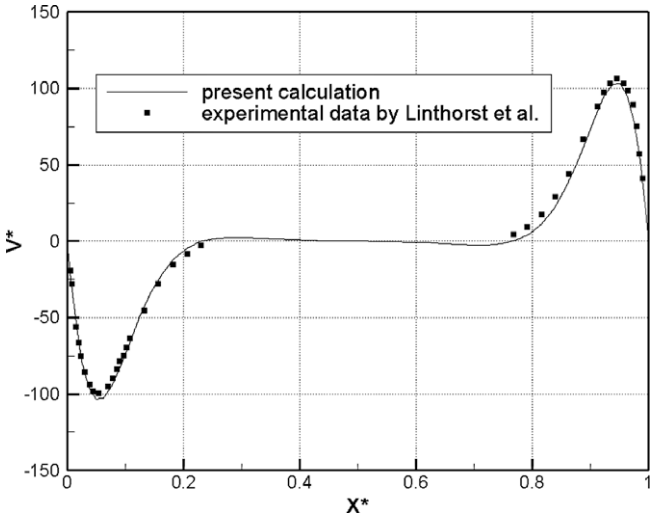

Fig. 3. Comparison of experimental data with dimensionless vertical velocities calculated along the mid-height of the cavity while Ra = 2.2×10^5 and Pr = 0.733.

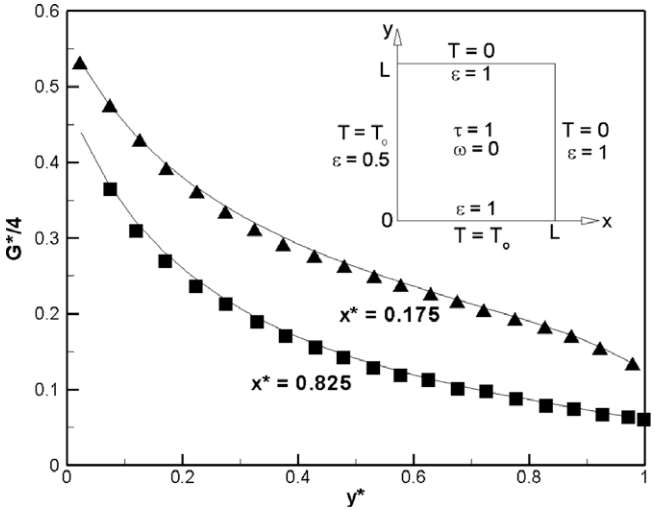

Fig. 5. Predicted dimensionless incident radiation at two representative locations in pure absorbing medium with $\tau = 1$ and $\omega = 0$.

medium can be found in Refs. [14,21] as well. Based on these validations, the present numerical method is applied to analysing the natural convection in the enclosure affected by combined radiation and an external magnetic field in the following.

4. Results and discussion

A numerical investigation is presented for natural convection of an electrically conducting and radiating fluid in a rectangular enclosure in the presence of a vertical magnetic field parallel to the gravity. The two opposing bounding surfaces of the enclosure are maintained isothermal, while one of the surfaces is cooled and the other is heated. Adiabatic conditions are imposed on two upper and lower bounding surfaces. Computations are carried out for the Grashof numbers ranging from 1×10^4 to 2×10^6, and Hartmann numbers from 0 to 100. The assumption of two-dimensional laminar flow is valid for above values of the Grashof number [22,23].

The physical model consists of a gray, absorbing, emitting, and non-scattering ($\omega = 0$) fluid in a cavity surrounded by rigid black walls. Basically three types of fluids are taking into account, which are opaque, transparent ($\tau = 0$), and participating ($\tau = 1$) fluids. Each fluid corresponds to the pure natural convection without radiation, natural convection with surface radiation only, and natural convection with surface and gas radiation, respectively.

It is difficult to study the influence of all parameters involved in the present problem on the flow and thermal field. Therefore a selected set of parameters is accounted for this numerical investigation. The aspect ratio, $A = H/L$, of the enclosure is set to be of 1, and the Prandtl number of 0.733 is utilised. The overheat ratio is taken to be $\delta = 2/3$, i.e., $T_H = 2\ T_C$. The constant fluid property and Boussinesq approximations are reasonable for above values [24,25]. The Planck number is assigned to be 0.02.

From Figs. 6–8, the effects of combined radiation and a magnetic field on the fluid flow and thermal fields, are displayed for different values of Ha. Isotherm and streamline plots are reported in those figures consecutively. The contour lines of isotherm plots correspond to equally-spaced values of the dimensionless temperature T^*, i.e., $\Delta T^* = 0.1$, in the range between -0.5 and $+0.5$. On the other hand the dimensionless stream function is obtained from the velocity field solution by integrating the integral

$$\Psi^* = \int_0^1 u^* dy^* \tag{24}$$

along constant x^* lines with $\Psi^* = 0$ at $x^* = y^* = 0$.

4.1. Influence of a magnetic field in case of an opaque fluid

To begin with, the radiative heat transfer in the fluid and between walls is neglected, which is the case for an opaque fluid, taking the Gr for 2×10^6. Fig. 6(a) exhibits the stratification of the temperature field in the vertical direction. The thermal boundary layer is well established along the thermally active side walls. At this high Grashof number, convection is the dominant heat transfer mechanism. The convection mainly affects the temperature distribution such that temperature gradients in the centre are close to zero. Strong upward flow arises near the heated wall and downward flow takes place at the cooled wall, as seen from the streamline pattern.

For a weak magnetic field with Ha = 10 as shown in Fig. 6(b), the flow and thermal fields don't display noticeable changes compared to the case of Ha = 0. As the Hartmann number reaches 50 for a moderate magnetic field, the temperature stratification in the core region begins to diminish. The isotherms in mid-region are inclined as illustrated in Fig. 6 (c). Furthermore the streamlines are elongated laterally and the axis of the streamline is tilted.

For a strong magnetic field with Ha = 100 as shown in Fig. 6(d), the axis of the streamline is severely inclined. The isotherms in mid-region are also seriously tilted. The convection is significantly suppressed owing to the strong retarding effect of the Lorentz force. The thermal boundary layers at two isothermal walls are died out, indicating the weakened role of the convection in heat transfer mechanism. Consequently the main effect of the introduction of a magnetic field is to reduce the overall heat transfer rate across the enclosure.

4.2. Effect of radiation in the absence of a magnetic field

Radiation-affected temperature and buoyant flow fields in a square enclosure are demonstrated with $Gr = 2 \times 10^6$, in the absence of an external magnetic field, i.e., Ha = 0. Those figures presented sequentially as Figs. 6(a), 7(a), and 8(a), are for opaque, transparent, and participating fluids, respectively.

In case the medium contained in a cavity participates in the absorption and emission of radiation, it can absorb radiant energy and transform it into thermal energy, thereby increasing the overall medium temperature compared with the non-radiative case. This is due to the so-called far-reaching effect of the radiation. Consequently, the medium temperature tends to be more uniform. Furthermore, as the participating medium attenuates the radiation more, a direct interaction between the hot and cold walls, i.e., surface radiation, is reduced.

The radiative interaction between the hot and cold walls is greater for the transparent fluid (Fig. 7 (a)), as the medium does not attenuate the radiation. The colder region ($T^* < 0$) is extended further into the mid-region. The temperature gradients at the adiabatic walls are steeper on account of the increased interaction by means of the surface radiation. The flow field displays a multi-cellular structure. The multi-cellular inner core consists of two convective rolls, which are designated by +'s, in the upper and lower halves, respectively.

On the other hand, for the participating fluid (Fig. 8 (a)), the temperature stratification in the centre region is not evident. Temperatures above the mean temperature ($T^* = 0$) take up most part of the enclosure due to the far-reaching effect. Colder region is restricted to the lower left part of the enclosure adjacent to the clod wall. The fluid motion becomes very intensive, and the flow pattern is drastically changed as well. The former multi-cellular inner core is destroyed and the strong unicellular flow is formed.

All the results discussed in this section confirm to prior investigation by Tan and Howell [26] qualitatively, which analysed combined radiation and free convection of a participating medium in a differentially heated square enclosure.

4.3. Effect of combined radiation and a magnetic field

The results depicted in Figs. 6 and 8, demonstrate the influence of the radiation on fluid flow and temperature distribution along with the magnetic field. They are presented together with constant buoyant action for $Gr = 2 \times 10^6$, otherwise stated.

Based on the results discussed in previous sections, the effects of combined radiation and a magnetic field are investigated in two ways. In the first place the effect of a magnetic field is examined for each radiating fluid in which the influence of Ha is evaluated in the framework of the same radiation environment. Secondly the variation in the thermo-fluid dynamics behaviour is observed in view of the radiation characteristics of fluids together with constant Ha.

Fig. 7 shows the variation in flow and thermal fields for the transparent fluid commensurate with the magnetic field strength.

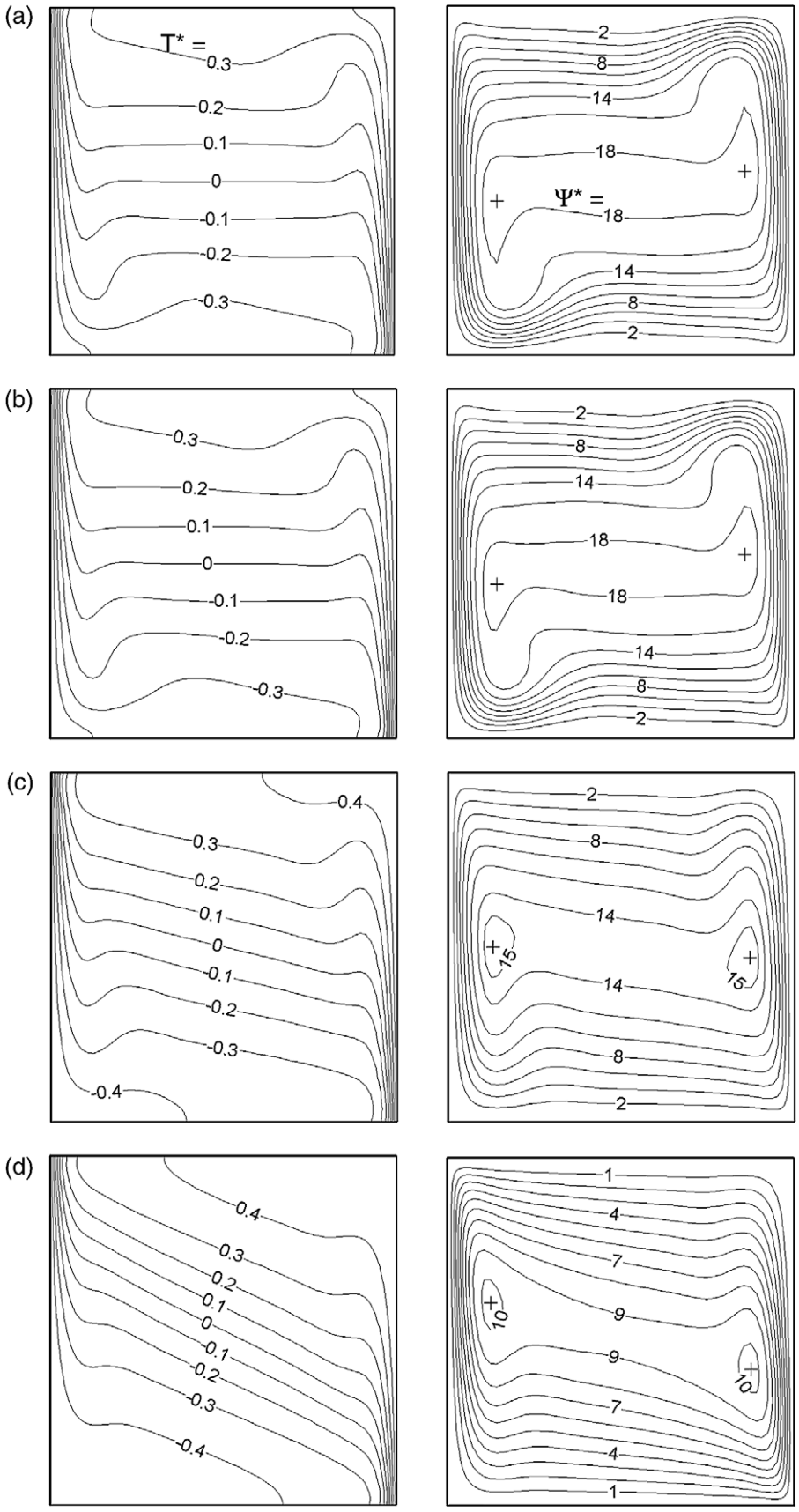

Fig. 6. Isotherm and streamline contours for the opaque fluid with $Gr = 2 \times 10^6$ and Pr = 0.733: (a) Ha = 0 ($\Delta\Psi^* = 2$); (b) Ha = 10 ($\Delta\Psi^* = 2$); (c) Ha = 50 ($\Delta\Psi^* = 2$); (d) Ha = 100 ($\Delta\Psi^* = 1$).

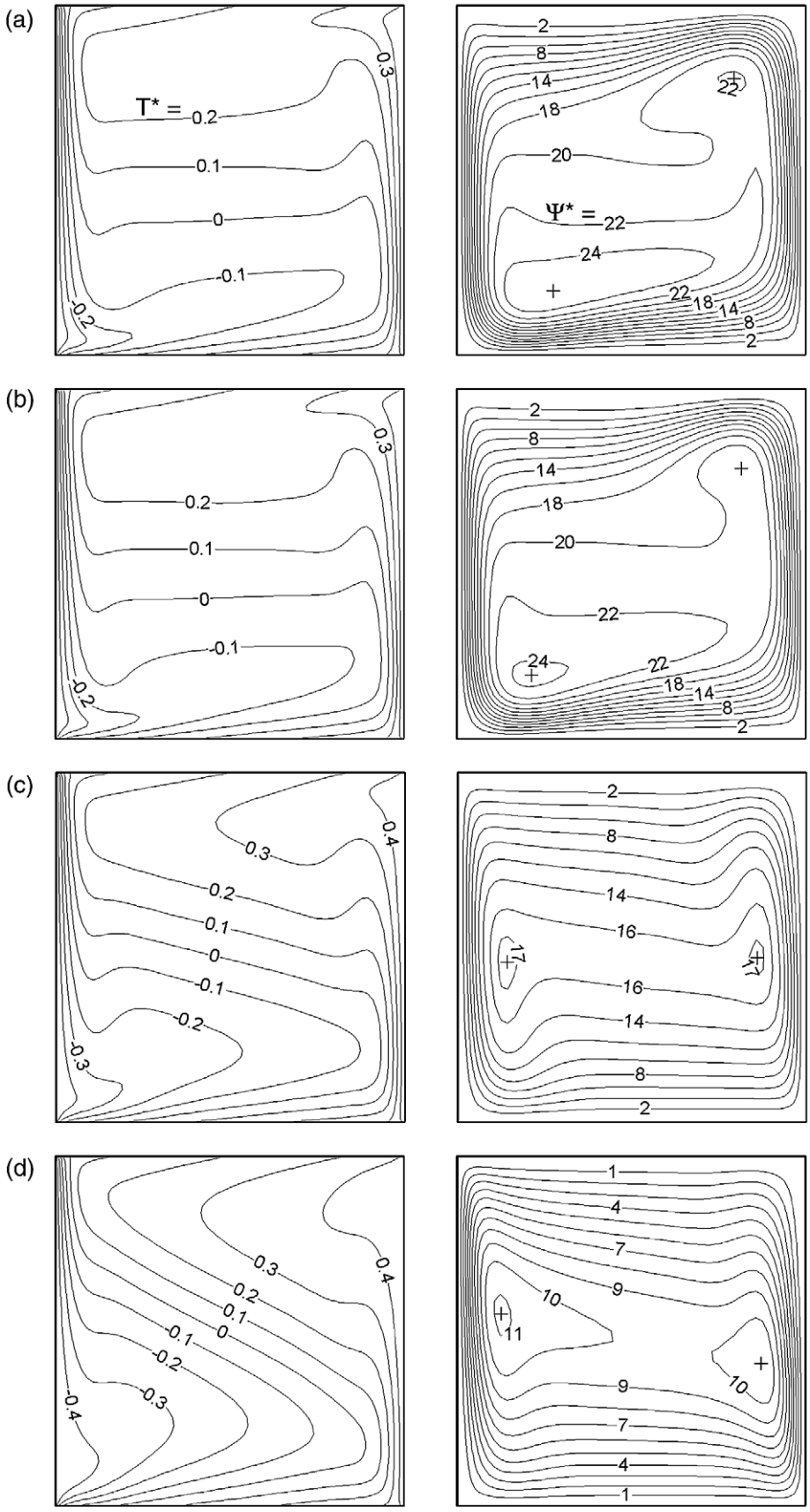

Fig. 7. Isotherm and streamline contours for the transparent ($\tau = 0$) fluid with Gr = 2×10^6, Pr = 0.733 and Pl = 0.02: (a) Ha = 0 ($\Delta\Psi^* = 2$); (b) Ha = 10 ($\Delta\Psi^* = 2$); (c) Ha = 50 ($\Delta\Psi^* = 2$); (d) Ha = 100 ($\Delta\Psi^* = 1$).

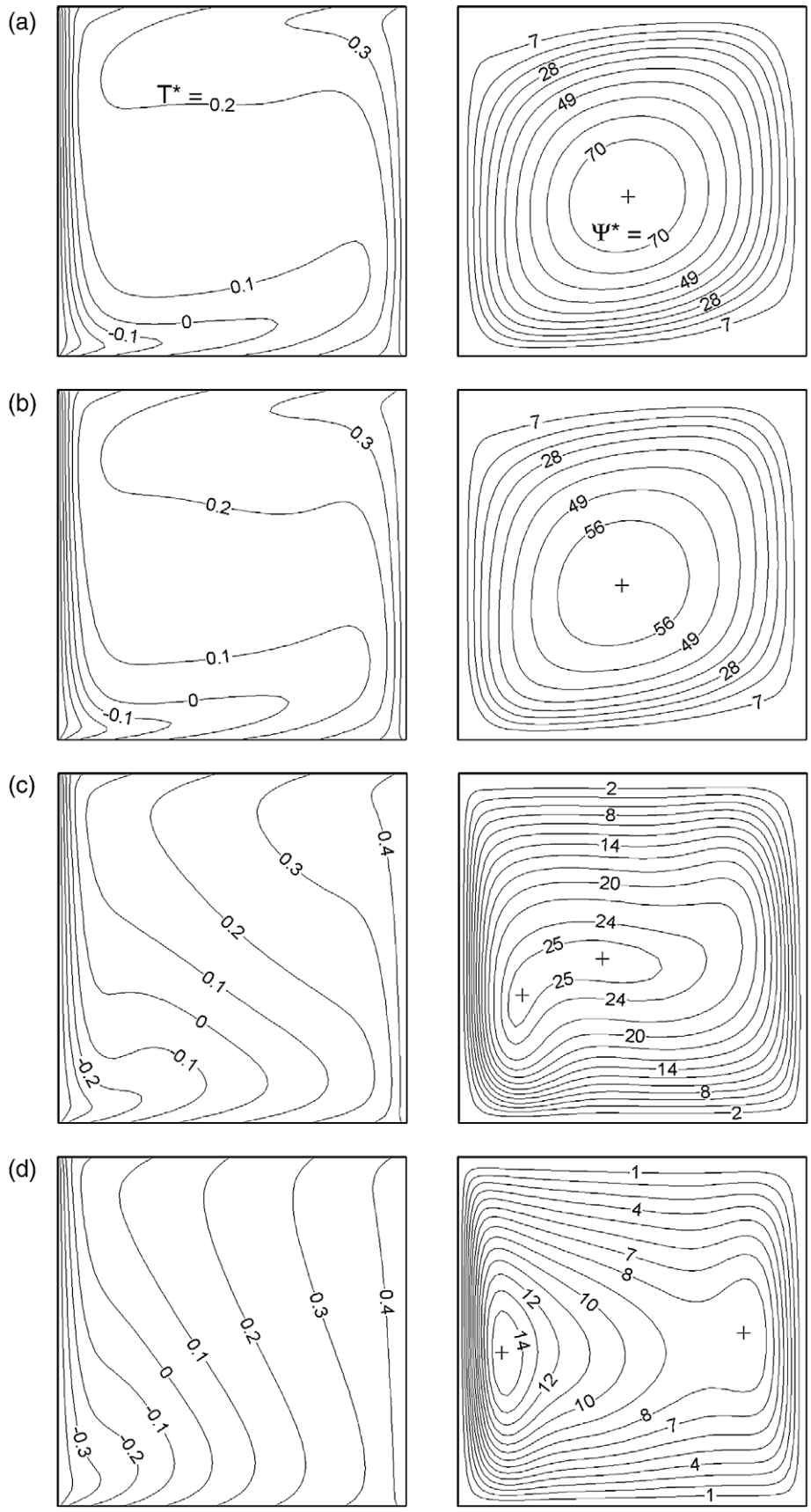

Fig. 8. Isotherm and streamline contours for the participating ($\tau = 1$) fluid with $Gr = 2 \times 10^6$, Pr = 0.733 and Pl = 0.02: (a) Ha = 0 ($\Delta\Psi^* = 7$); (b) Ha = 10 ($\Delta\Psi^* = 7$); (c) Ha = 50 ($\Delta\Psi^* = 2$); (d) Ha = 100 ($\Delta\Psi^* = 1$).

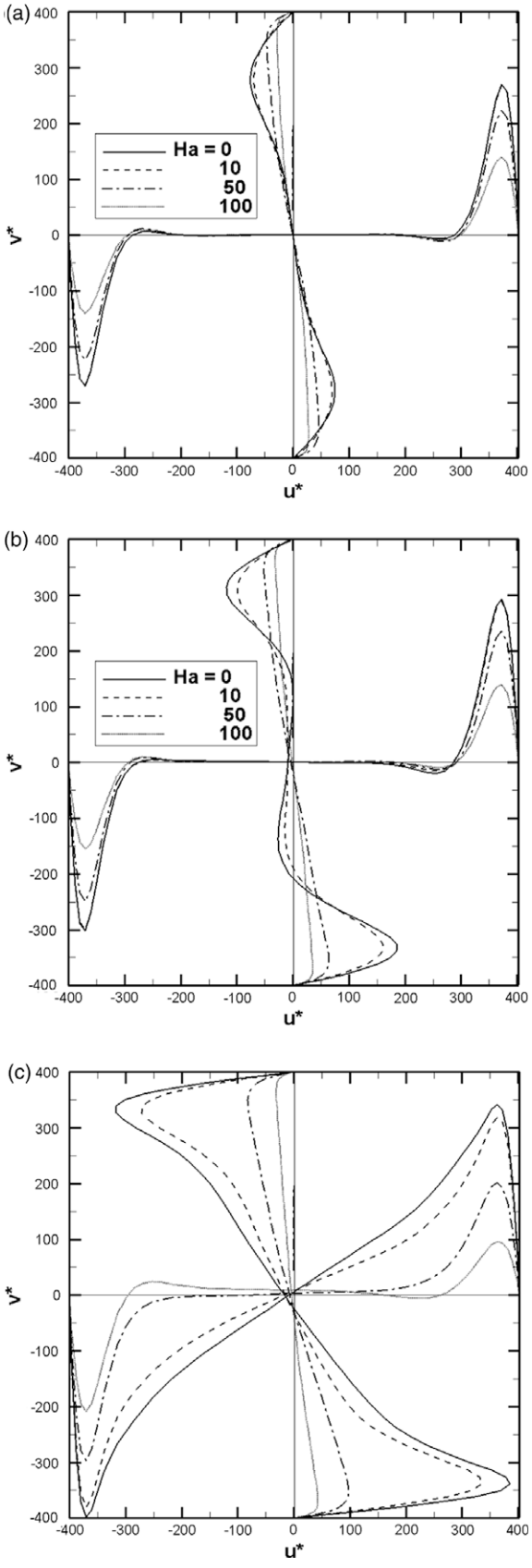

Fig. 9. Steady state dimensionless velocity components at mid-height and mid-width of the enclosure with Ha while $Gr = 2 \times 10^6$, Pr = 0.733 and Pl = 0.02: (a) opaque fluid; (b) transparent fluid, $\tau = 0$; (c) participating fluid, $\tau = 1$.

It is seen that for a weak magnetic field (Ha = 10), as shown in Fig. 7 (b), the isotherms and streamlines are almost similar to those in the absence of an external magnetic field. The flow field becomes less intensive a little bit than that corresponding to the streamline plot in Fig. 7(a). As a moderate magnetic field is applied, i.e., Ha = 50, the thermal and flow fields are considerably changed as depicted in Fig. 7(c). The streamlines are elongated laterally and the axis of the streamline is slanted. The former convective roll at the lower left part of the enclosure moves upward. On the contrary the convective roll which was at the upper right region moves downward as to increase in the strength of a magnetic field applied. In case of the thermal field, severe temperature gradients caused by the surface radiation are maintained at adiabatic top and bottom walls. In mid-region the tilting of isotherms coincides with steeper temperature gradient observed by in-between distance of isotherms getting narrower. These tendencies are preserved until Ha reaches 100 (Fig. 7(d)). Besides such typical influence of a magnetic field as the tilting of isotherms and streamlines, appears to be emphasised with the suppression of convection in an enclosure.

Fig. 8 displays the relative changes in thermo-fluid dynamics behaviour of the participating fluid relevant to the magnetic field strength. When applying a weak magnetic field with Ha = 10 (Fig. 8(b)), the colder region ($T^* < 0$) as well as the hotter region ($T^* > 0$) are extended more into the mid-region compared with the isotherms in Fig. 8(a). The overall configuration of streamlines seems to be invariant, though the flow intensity is considerably reduced. In terms of the case applying a moderate magnetic field, i.e., Ha = 50 (Fig. 8(c)), the multi-cellular inner core comes to appear, which is composed of two convective rolls. This phenomenon is caused by the applied magnetic field bringing about the lateral elongation of streamlines. The strength of the flow field is weakened and the tilting of isotherms emerges in parallel. The inclination of the streamline axis, however, is not happened in the present result, which was the distinctive effect of an external magnetic field applied in case of the non-participating fluids. If the Ha is increased up to 100 (Fig. 8 (d)), the multi-cellular inner core still exists, followed by apparent elongation of streamlines in the mid-region. The inner core comprises a strong primary convective roll adjacent to the left cold wall and a weak secondary convective roll in the vicinity of the right hot wall. The axis of the streamline is not tilted under the influence of this strong magnetic field. In contrast inclination of isotherms looks severe so that they tend to be parallel to the isothermal walls.

In the following the behaviour of radiating fluids is described with constant Ha. Discussions hereunder are based on the occasion of Ha = 50 concentrating on the sensible interaction of combined radiation and a magnetic field, referencing Figs. 6(c), 7(c) and 8 (c).

With applying the moderate magnetic field externally, the thermo-fluid dynamics behaviour in an enclosure is substantially altered in line with radiation effect. This can be observed in Fig. 7(c) for the transparent fluid in comparison with Figs. 6(c) for the opaque fluid. For the opaque fluid, the streamlines are elongated and the axis of the streamline is tilted, owing to the Lorentz force. Isotherms are inclined also, and they show the nearly symmetric distribution. In terms of the transparent fluid, however, the symmetricity of isotherms is broken down, and the hotter part of the temperature field ($T^* > 0$) extends more into the mid-region. Temperature gradients at ceiling and floor are increased by surface radiation, while the degree of tilting of isotherms in centre region is not changed considerably. It represents that the influence of the magnetic field on the temperature distribution remains dominantly in the mid-region, whereas the radiation effect is limited to the vicinity of the insulated walls. The overall flow intensity is

slightly strengthened compared to that of the opaque fluid flow, and a slant of the streamline axis is mitigated to some extent. But the global shape of the flow field has no significant difference from the opaque fluid flow.

On the other hand, when the fluid is participating in radiation, the resultant isotherms and streamlines display dissimilar pattern from prior results. In Fig. 8 (c), the isotherms in the mid-region are still inclined so that the influence of the external magnetic field on

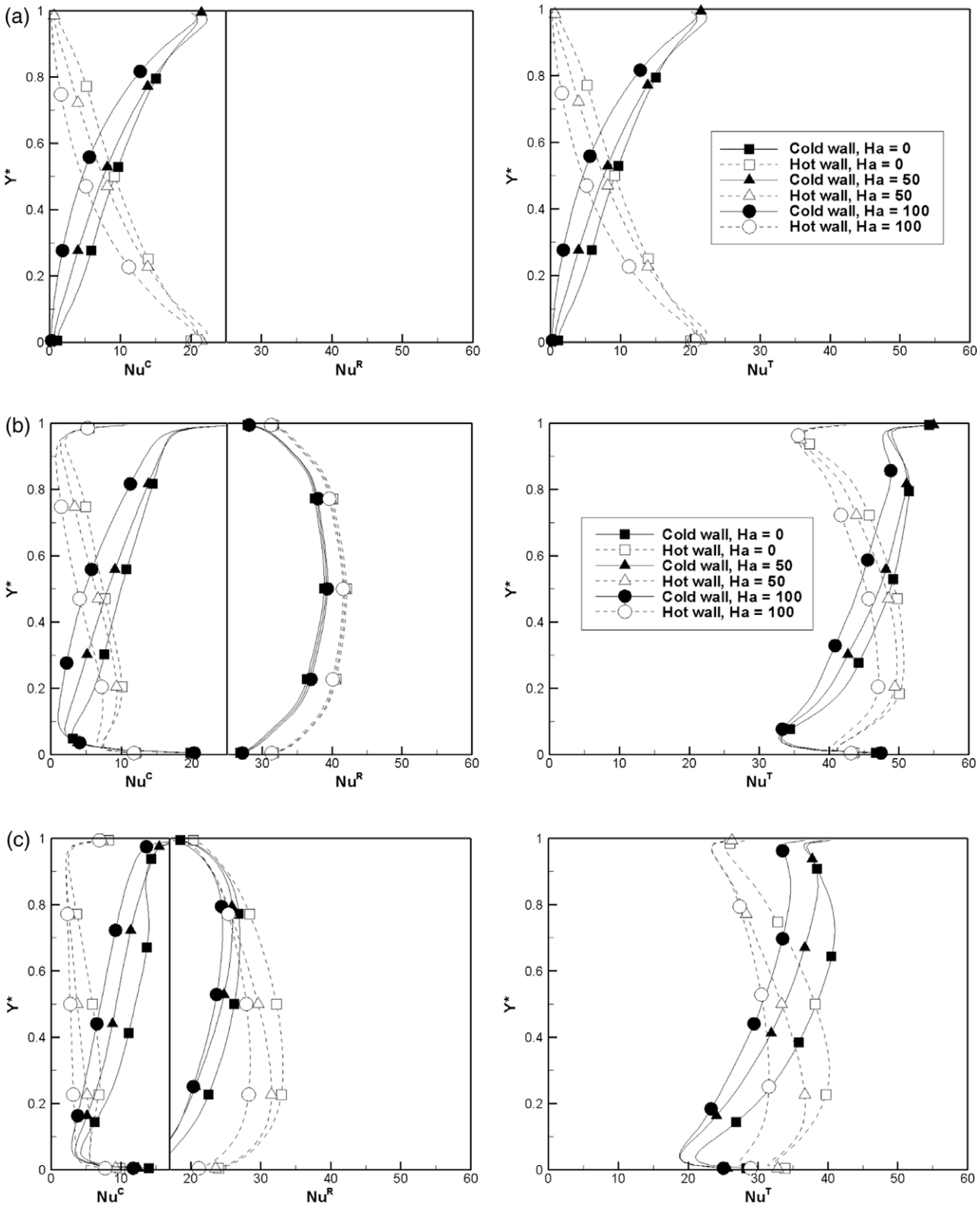

Fig. 10. Conductive, radiative and total local Nusselt number distribution at the hot and cold walls with Ha while Gr = 2×10^6, Pr = 0.733 and Pl = 0.02: (a) opaque fluid; (b) transparent fluid, $\tau = 0$; (c) participating fluid, $\tau = 1$.

them can be inferred. Besides the mean temperature ($T^* = 0$) migrates toward the lower left part of the enclosure because of the far-reaching effect of radiation forcing the medium temperature to be more uniform. As a result colder region is shrunken to the vicinity of the clod wall. The strength of circulating flows is linked to the thermal gradients, which are greater near the cooled wall than near the heated wall. It explains why the multi-cellular inner core moves leftward and is distorted seriously. Consequently the resultant thermal distribution for this fluid is strongly affected by not only the external magnetic field but radiation, even in the region far from the insulated walls. Temperature gradients at the adiabatic ceiling and floor become smoother than those for the transparent fluid, as the participating fluid attenuates more radiation than the transparent one. The overall flow intensity of the participating fluid is strongest among three fluids. The inclination of streamline axis vanishes on account of participation of the fluid.

The steady state dimensionless velocities at mid-height ($y^* = 0.5$) and mid-width ($x^* = 0.5$) of the enclosure are plotted for various values of Ha with respect to each radiating fluid, as depicted in Fig. 9. In case of the opaque fluid illustrated in Fig. 9(a), the horizontal velocity u^* perpendicular to a magnetic field, interacts directly with the magnetic field, and subsequently is suppressed seriously. The vertical velocity v^* parallel to a magnetic field, is also decreased appreciably by applying an external magnetic field. In a nutshell as the fluid is opaque, the increase in the magnetic field strength weakens overall velocities in flow field and flattens the velocity peak near the wall.

In the absence of a magnetic field, i.e., Ha = 0, the radiation effects are observed from both vertical and horizontal velocity profiles along the respective midplanes, in reference to Fig. 9(b) and (c). When the fluid is transparent, the inner core is rather stagnant. If the fluid participates in radiation, overall increase in the velocities is shown. Large velocity gradients occur along both thermally active and insulated walls.

Furthermore the effect of radiation on the changes in velocities is accounted for with non-zero Ha. As estimated from Fig. 9(b) and (c), the suppression of the velocity field by the magnetic field is apparent regardless of the radiation effect. The peak values of u^* and v^* are decreased rapidly as the Ha is increased. On the other hand it is observed that the downward flow at left cold wall is always stronger than the upward flow at right hot wall, especially for the participating fluid, regardless of Ha. It does explain the supplementary rationale for the fluid motion of that fluid displayed in Fig. 8. Moreover the velocities aligned to the insulated walls are such that the peak values of u^* over the floor is greater than those underneath the ceiling when Ha is small, whereas they become almost same if the Ha is increased over 50 as represented in Fig. 9(c). It is noteworthy that the stagnant inner core is restored regarding high Ha, in case of the participating fluid.

In Fig. 10 the conductive, radiative and total local Nusselt number distribution at the hot and cold walls is illustrated, depending on a type of the fluid. The distribution of conductive Nusselt number (Nu^C) at two isothermal walls is nearly symmetric for the opaque fluid as shown in Fig. 10(a). Concerning the transparent fluid in Fig. 10(b), difference in-between the radiative Nusselt number (Nu^R) distribution is rather small with variance of Ha. The participating fluid exhibits smaller magnitudes in the distribution of Nu^R at both isothermal walls, compared with those for the transparent fluid. It is caused by the attenuation of radiation when the radiant heat is transferring through the radiatively active medium. In addition the decrease in Nu^R is seen to be apparent following the increment of Ha, as displayed in Fig. 10 (c).

Basically regardless of a type of the fluid, the distribution of conductive Nusselt number is decreased at both hot and cold walls in accordance with the increase in Ha. A similar trend can be observed with the radiative Nusselt number distribution. As a consequence the increase in Ha leads to the decrease in the total local Nusselt number distribution, thereby resulting in the decrease of the total average Nusselt number eventually.

To explore the heat transfer characteristics of radiating fluids at steady state, a variation of the total average Nusselt number ($\overline{Nu}^T$) with Grashof number is plotted in Fig. 11 for several values of Ha. With constant Hartmann number, the increase of Grashof number is followed by the growth of $\overline{Nu}^T$, because of the rise in the relative magnitude of convective heat transfer. Moreover the effect of a magnetic field on the total heat transfer is such that the magnetic field reduces the total average Nu for any type of the fluid. Compared with other fluids, the participating fluid exhibits more variations in total heat transfer at high Grashof number according to the change of Ha.

As recognised from Fig. 10, radiation is the dominant mode of heat transfer and surpasses convective heat transfer, in case of the transparent and participating fluids. Furthermore as the optical thickness increases, more radiation is attenuated by the radiative medium in general. The comparative magnitudes of the total average Nu are, therefore, smallest for the opaque fluid, whereas they are largest for the transparent fluid, based on constant Gr.

The rate of heat transfer across the enclosure is attained by evaluating the conductive, radiative and total average Nusselt numbers, i.e., $\overline{Nu}^C$, $\overline{Nu}^R$ and $\overline{Nu}^T$, respectively, at the hot and cold walls, and tabulated in Table 1 for various combinations of parameters. To begin with, the values of the total average Nu obtained in the present study are compared to precedents for the pure free convection [27] as well as for the natural convection affected by an external magnetic field [3]. It is worth pointing out from the table that, especially when the Ha is of zero and the fluid is opaque, the values of $\overline{Nu}^T$ agree very well with those from the following correlation formula [27] which is considered as the benchmark solution in the range of Gr referenced in this study.

$$\overline{Nu}^C = 0.143(Gr \cdot \Pr)^{0.299}, \ 10^3 \le \mathrm{Gr} \cdot \Pr \le 10^6 \tag{25}$$

Besides the results of this study for the opaque fluid in the presence of a magnetic field are in good agreement with the published work available [3], as tabulated.

From this table it can be demonstrated that the introduction of a magnetic field suppresses the convection in the enclosure. As to the transparent and participating fluids, the radiative contribution to the combined heat transfer is predominant at both hot and cold walls. In addition the convective contribution to the combined heat

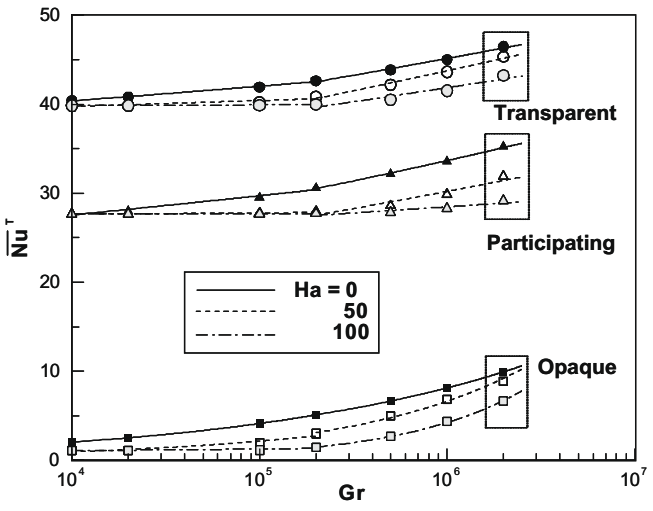

Fig. 11. Total average Nusselt number vs. Grashof number for radiating fluids affected by the external magnetic field while Pr = 0.733 and Pl = 0.02.

Table 1
Nusselt numbers.

Gr	Fluid types	Ha	Left cold wall		Right hot wall		$\overline{Nu}^T$		
			$\overline{Nu}^C$	$\overline{Nu}^R$	$\overline{Nu}^C$	$\overline{Nu}^R$	Present	Ref. [27]	Ref. [3]
2×10^4	Opaque	0	2.523	0.000	2.523	0.000	2.523	2.518	2.519
		10	2.220	0.000	2.220	0.000	2.220		2.223
		50	1.118	0.000	1.118	0.000	1.118		1.086
		100	1.116	0.000	1.116	0.000	1.116		1.011
	Transparent	0	4.049	36.733	2.105	38.678	40.783		
		10	3.754	36.759	1.874	38.641	40.513		
		50	3.021	36.841	1.368	38.494	39.862		
		100	2.997	36.846	1.357	38.487	39.843		
	Participating	0	5.638	22.340	2.626	25.352	27.978		
		10	5.528	22.252	2.592	25.189	27.780		
		50	5.439	22.222	2.574	25.088	27.661		
		100	5.436	22.223	2.574	25.086	27.658		
2×10^5	Opaque	0	5.090	0.000	5.090	0.000	5.090	5.012	4.920
		10	4.983	0.000	4.983	0.000	4.983		4.805
		50	2.997	0.000	2.997	0.000	2.997		2.844
		100	1.454	0.000	1.454	0.000	1.454		1.432
	Transparent	0	6.138	36.486	3.639	38.987	42.624		
		10	5.986	36.513	3.530	38.970	42.499		
		50	4.083	36.704	2.068	38.721	40.787		
		100	3.174	36.808	1.446	38.537	39.982		
	Participating	0	7.315	23.269	3.280	27.304	30.584		
		10	7.003	22.966	3.100	26.869	29.969		
		50	5.761	22.131	2.608	25.284	27.891		
		100	5.505	22.192	2.579	25.117	27.697		
2×10^6	Opaque	0	9.904	0.000	9.904	0.000	9.904	9.977	8.703
		10	9.863	0.000	9.863	0.000	9.863		8.646
		50	8.891	0.000	8.891	0.000	8.891		7.583
		100	6.640	0.000	6.640	0.000	6.640		5.542
	Transparent	0	10.413	36.047	6.946	39.514	46.460		
		10	10.339	36.073	6.914	39.499	46.412		
		50	9.025	36.313	6.050	39.289	45.338		
		100	6.699	36.531	4.178	39.054	43.230		
	Participating	0	11.240	23.986	5.284	29.942	35.225		
		10	11.158	23.892	5.224	29.827	35.050		
		50	9.397	22.490	3.939	27.950	31.888		
		100	7.473	21.664	2.894	26.243	29.138		

transfer at the cold wall is always larger than that at the hot wall disregarding the Grashof number and the fluid type.

5. Conclusions

A numerical investigation has been performed to investigate the effect of radiation on natural convection of an electrically conducting and radiating fluid in the presence of an external magnetic field aligned with gravity. Basically three types of fluids were considered, which were opaque, transparent and participating fluids. The results have been presented in the form of isotherms and streamline contour plots, mid-plane velocity profiles, and total heat transfer rates across the enclosure. The main conclusions of the present analysis are as follows:

- In case of the opaque fluid, the effect of an imposed magnetic field is to suppress the convection. If the fluid is not opaque in the absence of an external magnetic field, the flow structure and the temperature field in an enclosure are enormously affected by the radiation.
- In the framework of the same radiation environment, the thermo-fluid dynamics behaviour of a radiating fluid is substantially altered together with the strength of a magnetic field imposed. As for the transparent fluid, the effect of the magnetic field is the followings. In the mid-region apart from the adiabatic walls, the applied magnetic field affects the degree of tilting of a streamline axis appreciably. The radiation effect on a thermal field is localised near the adiabatic walls. In contrast the thermal distribution in the mid-region is affected by the magnetic field rather than the radiation. In terms of the participating fluid, as the magnetic field becomes stronger, the unicellular flow originally turns into the flow with the inner core including two convective rolls. The overall flow in the enclosure is suppressed by the retarding effect of the Lorentz force. Nevertheless the axis of the resulting streamline is not slanted even in the presence of a strong magnetic field. On the other hand the thermal distribution in the participating fluid is seriously affected by not only the external magnetic field but radiation, even in the region far from the insulated walls.
- In general terms, it is found that the main effect of the external magnetic field is to reduce the overall heat transfer rate across the enclosure. More specifically, regardless of a type of the fluid, the distribution of conductive Nusselt number is decreased at both hot and cold walls in accordance with the increase in the strength of a magnetic field imposed. A similar trend is observed with the radiative Nusselt number distribution. As a consequence the increase in Ha leads to the decrease in the total local Nusselt number distribution, thereby resulting in the decrease of the total average Nusselt number in the end.

Based on the results of this study specifying Pl = 0.02, it is concluded that the radiation is the dominant mode of heat transfer and surpasses convective heat transfer so that the radiation plays an important role in developing the hydromagnetic free convective flow in a differentially heated enclosure.

References

[1] M. Seki, H. Kawamura, K. Sanokawa, Natural convection of mercury in a magnetic field parallel to the gravity, J. Heat Transfer 101 (1979) 227–232.

[2] H. Ozoe, K. Okada, The effect of the direction of the external magnetic field on the three-dimensional natural convection in a cubical enclosure, Int. J. Heat Mass Transfer 32 (1989) 1939–1954.

[3] N. Rudraiah, R.M. Barron, M. Venkatachalappa, C.K. Subbaraya, Effect of a magnetic field on free convection in a rectangular enclosure, Int. J. Engng. Sci. 33 (1995) 1075–1084.

[4] R. Bessaih, M. Kadja, Ph. Marty, Effect of wall electrical conductivity and magnetic field orientation on liquid metal flow in a geometry similar to the horizontal Bridgman configuration for crystal growth, Int. J. Heat Mass Transfer 42 (1999) 4345–4362.

[5] L. Kolsi, A. Abidi, M.N. Borjini, N. Daous, H.B. Aissia, Effect of an external magnetic field on the 3-D unsteady natural convection in a cubical enclosure, Numer. Heat Transfer A 51 (2007) 1003–1021.

[6] A.J. Chamkha, Thermal radiation and buoyancy effects on hydromagnetic flow over an accelerating permeable surface with heat source or sink, Int. J. Engng. Sci. 38 (2000) 1699–1712.

[7] M.A. Seddeek, Effects of radiation and variable viscosity on a MHD free convection flow past a semi-infinite flat plate with an aligned magnetic field in the case of unsteady flow, Int. J. Heat Mass Transfer 45 (2002) 931–935.

[8] A.Y. Ghaly, Radiation effects on a certain MHD free-convection flow, Chaos, Solitons and Fractals 13 (2002) 1843–1850.

[9] A. Raptis, C. Perdikis, H.S. Takhar, Effect of thermal radiation on MHD flow, Appl. Math. Comput. 153 (2004) 645–649.

[10] S. Mahmud, R.A. Fraser, Analysis of mixed convection-radiation interaction in a vertical channel: entropy generation, exergy, Int. J. 2 (2002) 330–339.

[11] F.M. Modest, Radiative Heat Transfer, McGraw-Hill, 1993.

[12] S.V. Patankar, Numerical Heat Transfer and Fluid Flow, Hemisphere McGraw-Hill, Washington, DC, 1980.

[13] J.C. Chai, H.S. Lee, S.V. Patankar, Finite-volume method for radiation heat transfer, J. Thermophys. 8 (1994) 419–425.

[14] C.Y. Han, S.W. Baek, The effects of radiation on natural convection in a rectangular enclosure divided by two partitions, Numer. Heat Transfer A 37 (2000) 249–270.

[15] M.N. Borjini, L. Kolsi, N. Daous, H.B. Aissia, Hydromagnetic double-diffusive laminar natural convection in a radiatively participating fluid, Numer. Heat Transfer A 48 (2005) 483–506.

[16] M.N. Borjini, H.B. Aissia, K. Halouani, B. Zeghmati, Effect of optical properties on oscillatory hydromagnetic double-diffusive convection within semitransparent fluid, Int. J. Heat Mass Transfer 49 (2006) 3984–3996.

[17] S. Thakur, W. Shyy, Some implementational issues of convection schemes for finite-volume formulations, Numer. Heat Transfer B 24 (1993) 31–55.

[18] S.J.M. Linthorst, W.M.M. Schinkel, C.J. Hoogendoorn, Flow structure with natural convection in inclined air-filled enclosures, J. Heat Transfer 103 (1981) 535–539.

[19] F. Wolff, C. Beckermann, R. Viskanta, Natural convection of liquid metals in vertical cavities, Exp. Thermal Fluid Sci. 1 (1988) 83–91.

[20] J.C. Chai, A Finite-volume Method for Radiation Heat Transfer, Ph.D. thesis, University of Minnesota, Minneapolis, Minnesota, 1994.

[21] C.Y. Han, S.W. Baek, Natural convection phenomena affected by radiation in concentric and eccentric horizontal cylindrical annuli, Numer. Heat Transfer A 36 (1999) 473–488.

[22] S. Acharya, R.J. Goldstein, Natural convection in an externally heated vertical or inclined square box containing internal energy sources, J. Heat Transfer 107 (1985) 855–865.

[23] D.W. Larson, R. Viskanta, Transient combined laminar free convection and radiation in a rectangular enclosure, J. Fluid Mech. 78 (1976) 65–85.

[24] L.C. Chang, K.T. Yang, J.R. Lloyd, Radiation-natural convection interactions in two-dimensional complex enclosures, J. Heat Transfer 105 (1983) 89–95.

[25] T. Fusegi, B. Farouk, Laminar and turbulent natural convection-radiation interactions in a square enclosure filled with a nongray gas, Numer. Heat Transfer A 15 (1989) 303–322.

[26] Z. Tan, J.R. Howell, Combined radiation and natural convection in a two-dimensional participating square medium, Int. J. Heat Mass Transfer 34 (1991) 785–793.

[27] N.C. Markatos, K.A. Pericleous, Laminar and turbulent natural convection in an enclose cavity, Int. J. Heat Mass Transfer 27 (1984) 755–772.